A Demonstration of the Effects of Digitization on the Calculation of Kurtosis for the Detection of RFI in Microwave Radiometry

Roger D. De Roo, *Member, IEEE*, and Sidharth Misra

***Abstract*—Microwave radiometers detecting geophysical parameters are very susceptible to radio-frequency interference (RFI) from anthropogenic sources. RFI is always additive to a brightness observation, and so the presence of RFI can bias geophysical parameter retrieval. As microwave radiometers typically have the most sensitive receivers operating in their band, low-level RFI is both significant and difficult to identify. The kurtosis statistic can be a powerful means of identifying some types of low-level RFI, as thermal noise has a distinct kurtosis value of three, whereas thermal noise contaminated even with low-level nonthermal RFI often has other values of kurtosis. This paper derives some benign distortions of the kurtosis statistic due to digitization effects and demonstrates these effects with a laboratory experiment in which a known amount of low-level RFI is injected into a digital microwave radiometer.**

***Index Terms*—Detectors, digital radio, interference suppression, microwave radiometry.**

I. Introduction

RADIO-FREQUENCY interference (RFI) in microwave radiometry is both common and insidious. Such an interference has been documented at L-band [1], [2], C-band [3]–[6], X-band [6], [7], and, potentially, at K-band [8]. The prevalence of RFI at the lower frequencies of the microwave spectrum, where protected bandwidths are relatively small (or, for C-band, nonexistent), suggests that the powerful signal-processing capabilities of digital-receiver technology can be employed for RFI detection.

We previously reported an RFI detection technique which uses the kurtosis of the predetected voltage in a digital radiometer receiver to identify the presence of RFI. This technique has been demonstrated in the field [9], where the kurtosis statistic flagged many radiometric observations as being contaminated with RFI. These observations fell into two categories, one in which the brightness observations were too large to be from a thermal origin, and so the kurtosis-based identification was confirmed, and the other in which the brightness observations were not obviously increased by RFI. Without precise knowledge of the radio environment in which this receiver was operating, it is impossible to precisely quantify the ability of the kurtosis statistic to flag RFI from the measurements. Therefore, a study was conducted to predict the performance of the kurtosis statistic as a means of identifying pulsed sinusoidal RFI [10]. This paper presents the results of a laboratory experiment in which a known level of pulsed sinusoidal RFI is injected into a microwave radiometer with a digital receiver to validate the predictions of the theoretical study. We found that the predictions are largely supported, but small modifications of the theory are required to account for the methodology of the measurements.

The next section provides a brief review of the kurtosis statistic as applied to radiometric RFI detection. Section III describes the laboratory experiment, and Section IV compares the measurements of large RFI contributions with the theory as previously developed. In Section V, an extension of the theory for the kurtosis statistic is developed to account for the effect of the finite span of the analog-to-digital converter (ADC) on the calculation of the kurtosis. In Section VI, the span and resolution of the digitizer in the receiver are artificially varied to evaluate this effect. In Section VII, a further extension of the theory is derived to account for some limitations of the measurement apparatus, which cause a small reduction of the calculated kurtosis. This small reduction is confirmed with the measurements of small RFI contributions in Section VIII, before we conclude this paper in Section IX.

II. Kurtosis Statistic and RFI

A. Voltage PDF of Noise With No RFI

The kurtosis R of the predetected voltage v is defined as the fourth central moment m_4 divided by the square of the second central moment m_2 [11]

$$R = \frac{m_4}{m_2^2} \tag{1}$$

where $m_p = \langle (v - \langle v \rangle)^p \rangle$ and $\langle \cdots \rangle$ denotes the expected value. The calculation of (1) requires the probability density function (pdf) of v. For a radiometric observation that only includes

Manuscript received October 1, 2007; revised November 1, 2007 and December 11, 2007. Current version published October 1, 2008. This work was supported in part by the NASA SBIR Program under Contract NNG06CA27C and in part by the NASA Earth Science Technology Office under Grant NNG05GL97G.

The authors are with the Department of Atmospheric, Oceanic, and Space Sciences, University of Michigan, Ann Arbor, MI 48109 USA (e-mail: deroo@umich.edu).

Color versions of one or more of the figures in this paper are available online at http://ieeexplore.ieee.org.

Digital Object Identifier 10.1109/TGRS.2008.916483

amplified scene brightness and receiver noise, the contributing mechanisms are purely thermal, and the pdf is Gaussian [12]

$$p_g(v) = \frac{1}{\sqrt{2\pi}\sigma} \exp(-v^2/2\sigma^2) \tag{2}$$

where σ^2 is the variance of the noise, and is related to the power at the radiometer digitizer: $\sigma^2/Z_0 = kT_{\mathrm{SYS}}BG$, where Z_0 is the impedance of the matching circuit at the digitizer, k is the Boltzmann constant, T_{SYS} is the radiometer system temperature, B is the radiometer bandwidth, and G is the radiometer gain prior to digitization. For pure Gaussian noise, $R = 3$.

B. Voltage PDF of RFI With No Noise

While RFI takes many forms, we will assume in this analysis that it takes the form of a pulsed sinusoid. For a sinusoid of amplitude A, the pdf is $p_{\sin}(v) = 1/(\pi\sqrt{A^2 - v^2})$ [13]. When pulsed with duty cycle d, the pdf of this RFI is given by

$$p_{\mathrm{ps}}(v) = (1-d)\delta(v) + \frac{d}{\pi\sqrt{A^2 - v^2}} \tag{3}$$

where $\delta(x)$ is the Dirac delta function.

This form of the RFI is expected to be representative of radar pulses and, when $d = 1$, for broadcast carriers. In a digital receiver, we are assuming that the samples of the pulsed sinusoid are uniformly random in phase. As long as this condition holds, the pulsed sinusoidal RFI may appear either in-band or out-of-band. While amplitude modulation of the sinusoid will distort the pdf away from the idealization of (3), to first order, phase and frequency modulation will not.

C. Voltage PDF of Noise With RFI

The radiometer digitizes the combined waveform of (2) and (3) when pulsed sinusoidal RFI is present. Rice [14] derived the pdf for the instantaneous voltage of a sinusoid contaminated with Gaussian noise. His expression is easily extended to the case of Gaussian noise contaminated by a pulsed sinusoid [10]

$$\begin{aligned} p(v) &= p_g(v) \otimes p_{\mathrm{ps}}(v) \\ &= \frac{1}{\sqrt{2\pi}\sigma} \exp(-v^2/2\sigma^2) \\ &\quad \times \left(1 + d\sum_{k=1}^{\infty} \frac{1}{(k!)^2} \left(\frac{A}{2\sigma}\right)^{2k} \mathrm{He}_{2k}\left(\frac{v}{\sigma}\right)\right) \end{aligned} \tag{4}$$

where $\otimes$ indicates convolution and $\mathrm{He}_{2k}(x)$ is a Hermite polynomial of even order [15]. This expression readily yields the second and fourth moments of the pulsed sinusoidal RFI-contaminated predetected voltages [10]

$$m_2^a = \sigma^2(1+S) \tag{5}$$

$$m_4^a = 3\sigma^4\left(1 + 2S + \frac{1}{2d}S^2\right) \tag{6}$$

where $S = dA^2/2\sigma^2$ is the average sinusoid-to-noise ratio, and quantifies the RFI contamination in a brightness measurement. The superscript a indicates that these moments apply to the analog voltage just prior to digitization. Thus, in the absence of RFI, the kurtosis $R = 3$, whereas $R > 3$ for short sinusoidal pulses and $R < 3$ for continuous-wave (CW) RFI. The kurtosis is blind to RFI at a 50% duty cycle.

The RFI-free kurtosis calculated from analog moments has been shown to be statistically independent from the estimate of the variance [11]. Thus, the kurtosis can be an unbiased detector of RFI.

III. Experimental Setup

To demonstrate the capabilities of the kurtosis statistic for RFI detection, a benchtop digital radiometer has been constructed into which a controlled sinusoidal pulse is injected. A block diagram of this radiometer is shown in Fig. 1. A pulsed sinusoid is created in an Agilent N6030A arbitrary waveform generator (AWG), which is part of an L-band version of the Correlated Noise Calibration Standard (CNCS) [16]. One CNCS L-band RF head is switched between a 303.9-K background from a reference load and a 73.3-K background ColdFET [17]. The pulsed sinusoid is injected on top of the ColdFET brightness. The AWG is programmed to create a pulsed sinusoid at 320.75 MHz with 0.1%, 1%, 10%, 50%, and 100% duty cycles. The pulse repetition period is 6.4 ms in all cases. The pulsed-sinusoid amplitude is controlled with attenuators, in 6-dB steps, inserted at the AWG output prior to upconversion within the RF head to 1412.75 MHz.

The analog front end of this benchtop radiometer is provided by the RFI Detection and Mitigation Testbed [18], in which the RF is filtered to a 20-MHz bandwidth and downconverted to an intermediate frequency (IF) centered at 27 MHz. This analog portion of the benchtop radiometer is not thermally controlled. The digital back end is provided by the Agile Digital Detector (ADD) [9], which digitized the incoming IF at a resolution of 8 bits and a rate of 110 MSa/s. The data are processed in an onboard field-programmable gate array (FPGA). While it is a simpler operation to directly generate moments, this firmware counts the number of occurrences of each digitized level in every 36-ms integration period to permit more thorough explorations of the effects of RFI. The ADD FPGA also performed this same histogram-generating operation on eight subbands, each of which being 3 MHz wide. The pulsed sinusoid falls within the passband of subband 5 and 0.75 MHz outside of subband 4. In this paper, we explore the data from subband 5 only.

IV. Deflection of Kurtosis Due to RFI

Fig. 2 shows some examples of the output of the ADD receiver, which is a count of the number of events in each digitizer bin for subband 5 during each integration period. In this particular example, the pulsed sinusoid is at its maximum amplitude that does not saturate the ADC. We attribute the minor discrepancies in the match of the data to the expected

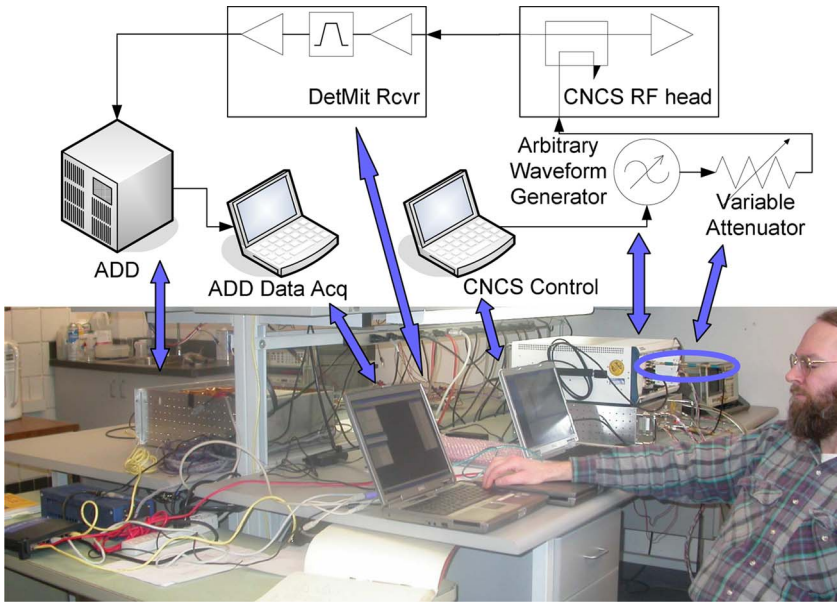

Fig. 1. Setup of benchtop radiometer into which known levels of pulsed sinusoidal RFI were injected. The CNCS RF head is behind the AWG.

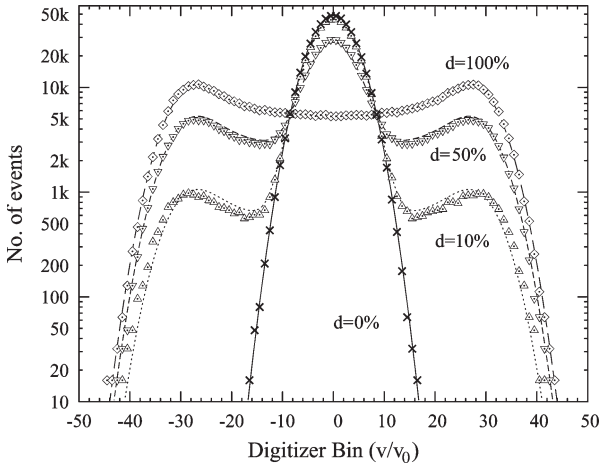

Fig. 2. Histograms of the instantaneous voltage collected with the benchtop radiometer and compared to the theory. The marks represent histogram bin count data, whereas the curves denote the predictions of (4). In all cases, $\sigma = 4.08v_0$ and, for the curves with nonzero duty cycle, $A = 39.92v_0$. The $d = 0$ curve is a Gaussian pdf. Each histogram represents one integration period and contains about 495 000 events.

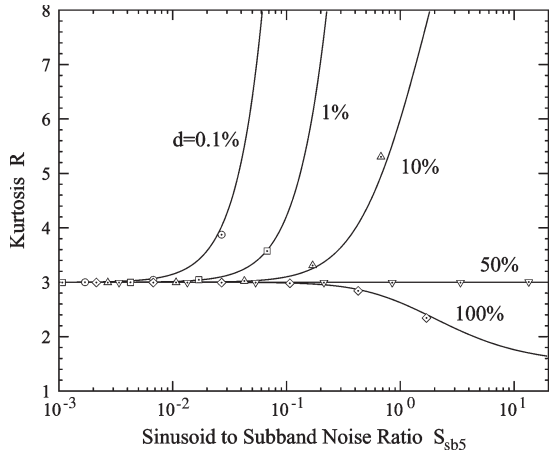

Fig. 3. Kurtosis as a function of pulsed sinusoidal duty cycle and integrated sinusoid-to-noise ratio. The data points are averages of kurtosis calculated from ADD histograms, and the curves are the kurtosis calculated from (5) and (6).

distribution, given by (4), to gain drifts in the thermally uncontrolled portion of the benchtop radiometer. In this instance, the RFI-induced deviation from a Gaussian distribution, which is included in the figure, is obvious. At lower duty cycles and lower pulsed-sinusoid amplitudes, the differences between (2) and (4) cannot be easily seen graphically.

Fig. 3 shows the mean kurtosis statistics calculated from the ADD histogram data. The kurtosis is calculated from each integration period and averaged over 5 min of data collection (approximately 8225 integration periods). As the sinusoid-to-noise ratio S decreases, the kurtosis approaches the RFI-free value of $R = 3$. The kurtosis for CW sinusoids is decreased from this value. The kurtosis value for pulsed sinusoids is larger than three, with the deviation becoming stronger as d decreases. For a given S, the amplitude A must be larger at lower duty cycles. A strong amplitude contributes to longer tails of the distribution, thus generating a large kurtosis. The kurtosis of noise with 50% duty cycle sinusoid is indistinguishable from RFI-free kurtosis despite the obvious differences in the probability distribution function seen in Fig. 2. This is because the kurtosis is not a complete description of a probability density distribution. More moments can be used to identify RFI in this case, but we do not expect sinusoids that are present during 50% of an integration period to be very common. At this scale, the analog expression for the kurtosis is adequate to demonstrate the ability of the kurtosis to predict the presence of relatively large contributions of RFI to the brightness.

V. ADC Effects on Kurtosis

The act of digitizing affects the calculation of the variance and kurtosis in two ways. The first effect of digitizing is an

increase of the second and fourth central moments due to the finite bin size [19]

$$m_2^d = \frac{m_2^a}{v_0^2} + \frac{1}{12} \tag{7}$$

$$m_4^d = \frac{m_4^a}{v_0^4} + \frac{1}{2}\frac{m_2^a}{v_0^2} + \frac{1}{80} \tag{8}$$

where v_0 is the bin size of the ADC. These expressions are valid as long as $\sigma > 3/4\ v_0$; otherwise, the null offset in the ADC must be included [19].

The second effect is due to the finite span of the ADC. Radiometry, in the absence of RFI, benefits from increased bandwidth because the product of bandwidth and integration time reduces the radiometric uncertainty. When increasing digital bandwidth, it is desirable to reduce the number of bits in the ADC to keep the overall data rates in the digital receiver from becoming very large. However, the finite span can result in distortion of the observed pdf due to saturation (the assignment of samples beyond the span of the ADC to the nearest extreme ADC level) or clipping (the discarding of those samples).

For an ADC with an odd number of levels, $2L+1$, the saturated pth moments are given by [11]

$$m_p^{\text{sat}} = 2\left(\sum_{k=1}^{L} k^p P(k) + \sum_{k=L+1}^{\infty} L^p P(k)\right) \tag{9}$$

$$= 2\left(\sum_{k=1}^{\infty} k^p P(k) - \sum_{k=L+1}^{\infty} k^p P(k) + L^p \sum_{k=L+1}^{\infty} P(k)\right) \tag{10}$$

where

$$P(k) = \int_{(k-\frac{1}{2})v_0}^{(k+\frac{1}{2})v_0} p(v)dv \tag{11}$$

is the probability of an event occurring in bin k of an infinite-span ADC with the center of bin 0 at $v = 0$ and bin size v_0. The first sum of (10) is given by (7) and (8). Because we are particularly interested in the behavior of the digitized moments when RFI contributions are small, we will assume for the other two sums that $p(v) \approx p_g(v)$. Then, the third sum can be evaluated exactly, and the second sum can be approximated with an integral. The results are

$$m_2^{\text{sat}} = m_2^d - s^2\left(1 - \text{erf}(z) + \frac{2z}{\sqrt{\pi}}e^{-z^2}\right) + L^2\left(1 - \text{erf}(z)\right) \tag{12}$$

$$m_4^{\text{sat}} = m_4^d - 3s^4\left(1 - \text{erf}(z) + \frac{2z}{\sqrt{\pi}}\left(1 + \frac{2z^2}{3}\right)e^{-z^2}\right) + L^4\left(1 - \text{erf}(z)\right) \tag{13}$$

where $s = \sigma/v_0$ is the radiometric signal strength normalized to the ADC bin size, and

$$z = \frac{2L+1}{2\sqrt{2}s} \tag{14}$$

is a measure of where, on the Gaussian distribution, the saturation is occurring.

For clipping instead of saturation, the final term, proportional to L^p, should be dropped

$$m_2^{\text{clip}} = m_2^d - s^2\left(1 - \text{erf}(z) + \frac{2z}{\sqrt{\pi}}e^{-z^2}\right) \tag{15}$$

$$m_4^{\text{clip}} = m_4^d - 3s^4\left(1 - \text{erf}(z) + \frac{2z}{\sqrt{\pi}}\left(1 + \frac{2z^2}{3}\right)e^{-z^2}\right). \tag{16}$$

Numerical simulations indicate that these equations are valid for $z > \sqrt{2}$, i.e., an ADC span which is greater than 4σ.

VI. Reprocessing of Measured Data to Mimic ADC Finite Span

Since the data collected by the ADD instrument is event counts for each digitized level, it is possible to post-process this data in such a way to explore the effects of ADC finite span. Fig. 4 shows two independent reprocessing operations on some data: reducing the bin, L, at which saturation occurs, and increasing v_0, the size of the bins. These operations are performed on a set of data collected by ADD when looking at both the reference load and ColdFET, and the reprocessed data are shown in Fig. 5.

The ADC effects manifest themselves in the values of the kurtosis as a decrease of the kurtosis from three even for RFI-free observations. Below $s = 1$, the reduction in kurtosis for all the curves is due to the fact that the observations are being sampled too coarsely. In other words, the radiometer gain is too low. As s increases to the point that saturation occurs, the kurtosis again dramatically drops. Saturation in the absence of RFI constitutes a nonlinear and less sensitive measurement of brightness. For detecting RFI, saturated data (data which would have been in the tail of the histogram) is difficult to distinguish between the desired noise signal or the undesired RFI, reducing the effectiveness of the kurtosis statistic as a detector of RFI. For both of these reasons, saturation of any expected brightness observations should be avoided.

From the figure, we can see that, as s increases, the calculation of kurtosis asymptotically approaches three. However, when s exceeds about 10% of the span, the kurtosis decreases due to the accumulation of events in the last bins ($\pm L$). This figure suggests that, to use the kurtosis statistic as detector of RFI, with known performance, the ADC should have at least four bits. With an ADC with fewer bits, the kurtosis threshold for RFI may need to be a function of brightness, or, for a fixed threshold, the sensitivity of the kurtosis to RFI will depend on the brightness. A dynamic kurtosis threshold defeats an advantage of the kurtosis method, namely, its statistical independence from the variance.

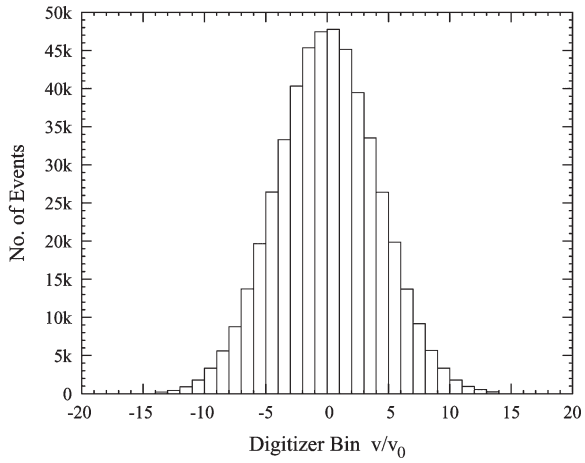

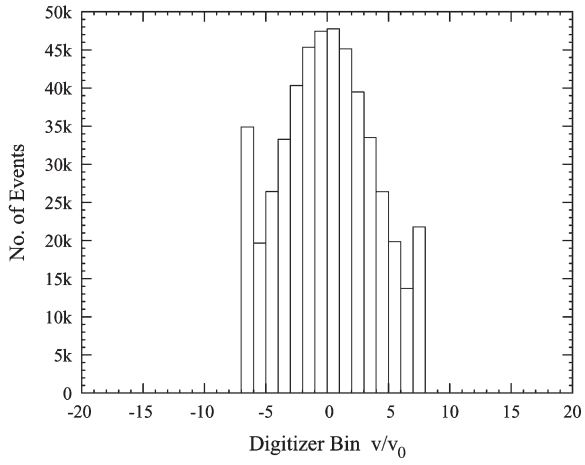

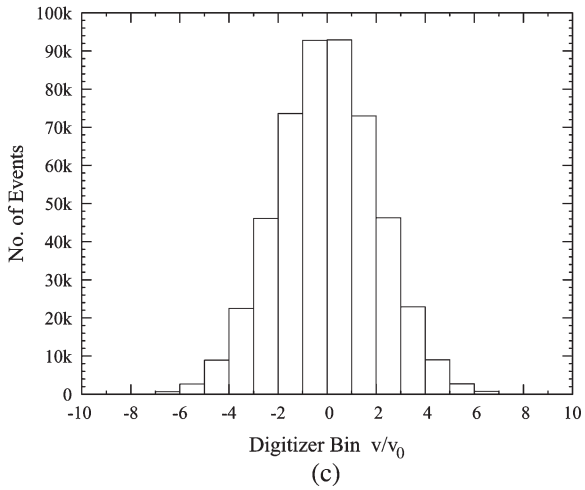

Fig. 4. Data reprocessing operations for evaluation of effects of ADC bin size and span. (a) The original histogram collected by ADD when looking at a 73-K ColdFET with no added RFI. (b) Histogram in (a) saturated at $L = \pm 7$. (c) Histogram in (a) with a doubling of the bin size (v_0). Both the horizontal and vertical axes of (c) have changed by a factor of two over that in (a). Both of these operations are used together to produce the next figure.

VII. Effects of Truncated Event Counts

The firmware used in the experimental setup of Section III is a legacy of an earlier ADD demonstration of RFI detection in close proximity to an air traffic control radar [9]. In this

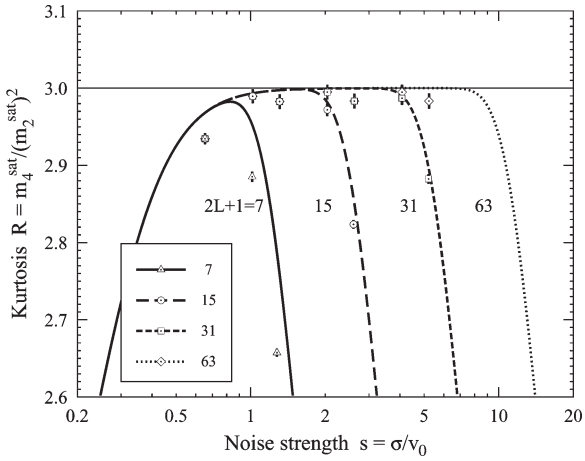

Fig. 5. Kurtosis of RFI-free observations as affected by ADC bin size (through the signal strength $s = \sigma/v_0$) and ADC span $2L + 1$ at 7, 15, 31, and 63 levels. Events occurring beyond the ADC span are accumulated in the last bins $(\pm L)$. Both the curves, given by (12) and (13), and the marks converge as s decreases. The ADC must have more than 3 bits for the kurtosis to have minimal sensitivity to the brightness.

firmware, the resolution of event counts was reduced by truncating the three least significant bits (LSBs) of the full-band event counts and four LSBs of each of the subbands. This reduction in resolution permitted a shorter integration period than would otherwise be possible by reducing the back-end data offloading requirements.

To explore the limits of sensitivity of the kurtosis statistic, we need to describe the behavior of the kurtosis for very small amounts of RFI contamination. Unfortunately, the kurtosis, as calculated from the RFI-free data gathered by the ADD when rounding the event counts, is consistently around 2.995, even though the earlier analyses indicate that it should be much closer to three. When the event counts are truncated, the RFI-free kurtosis is around 2.976. In this section, we will explore the effects of the histogram truncation in ADD and show that this explains the behavior of the mean value of the kurtosis at small contributions of RFI. Even though this effect is unique to the way in which these data were collected, an adequate explanation of observations permits confidence in the method of RFI detection using the kurtosis.

For the measurements described in Section III, the number of events in each bin is rounded off to the nearest $2^4 = 16$ prior to the offloading operation. We have also collected some data for which the four LSBs are dropped without rounding first. This event count truncation or rounding has its own two effects on the calculation of the kurtosis. First, the tails of the histogram are cut off, and second, the number of events in nonempty bins is altered from the actual number that occurred.

A. Tail Trimming

When the LSBs of a histogram bin are truncated, the tails of the distribution are cut off. The likely bins in the tail of the histogram to experience trimming are those that are expected to contain fewer than $N_{\rm et} = 2^n$ events, where n is the number of LSBs truncated. For rounding, this threshold is $N_{\rm er} = 2^{n-1}$.

Note that, for 1-bit rounding, the tails of the distribution are not trimmed: Only those bins with no events are reported as empty.

The number of events, N_e, expected in a bin k is given by

$$\langle N_e \rangle = N \cdot P(k) \approx \frac{N}{\sqrt{2\pi}s} \exp\left(-k^2/2s^2\right) \tag{17}$$

where N is the total number of events in the pristine histogram (i.e., prior to truncation or rounding). Because we are interested in weak or nonexistent RFI, $P(k)$ is approximated as coming from a purely Gaussian process. Also, the noise distribution is assumed sufficiently strong $(s > 1)$ such that the approximation is very good and that any null offset in the ADC is negligible.

Let $L_{\rm et}v_0$ be the voltage at which the expected number of events in a bin of width v_0 is $N_{\rm et}$. By equating $N_{\rm et}$ and $\langle N_e \rangle$, we can solve for $k = L_{\rm et}$, the center of the "bin" at which the histogram tails are being cut off due to truncation

$$L_{\rm et} = \sqrt{2s^2 \ln\left(\frac{N/N_{\rm et}}{\sqrt{2\pi}s}\right)}. \tag{18}$$

A similar result for $L_{\rm er}$ is obtained by substituting the subscript er for et in the aforementioned equation. Two voltages satisfy this condition: $-L_{\rm et}v_0$ and $+L_{\rm et}v_0$. The effect of this tail trimming can be then modeled with (15) and (16), with $L_{\rm et}$ or $L_{\rm er}$ being used for L in (14). While tail trimming for a particular histogram takes place at the edge of a bin, which is given by an integer, $L_{\rm et}$ or $L_{\rm er}$ should be real in recognition of the variability of the actual bin at which tail trimming occurs over an ensemble of histogram realizations.

B. Event Count Distortion

During truncation, the number of events in bins from $-L_{\rm et}$ to $+L_{\rm et}$ is altered. For each nonempty bin, the number of reported events is the actual number of events integer divided by 2^n. When reconstituted, by multiplying with 2^n in postprocessing, the difference from the original event count is uniformly distributed from 0 to $2^n - 1$, except when very close to the extreme bins containing $\pm L_{\rm et}v_0$. The assumption of uniformity is appropriate because the number of events in the middle bins should be very large compared to 2^n. When truncated, the average increase in the number of events, $\Delta N_{\rm et}$, is the negative of the sum of all possible reductions (uniformly weighted)

$$\langle \Delta N_{\rm et} \rangle = -\frac{1}{2^n} \sum_{k=0}^{2^n-1} k = -\frac{1}{2}(2^n - 1). \tag{19}$$

For rounding, the effect is similar, except that the increase in the number of events ranges uniformly from $1 - 2^{n-1}$ to 2^{n-1}. Thus, the average increase in the number of events per bin when rounded is

$$\langle \Delta N_{\rm er} \rangle = \frac{1}{2^n} \sum_{k=1-2^{n-1}}^{2^{n-1}} k = \frac{1}{2}. \tag{20}$$

TABLE I
EXAMPLE OF EVENT COUNT DISTORTION DUE TO TRUNCATION AND ROUNDING

k	N_e	ΔN_{et}	ΔN_{er}
10	2431	-15	+1
11	1298	-2	-2
12	653	-13	+3
13	309	-5	-5
14	138	-10	+6
15	58	-10	+6
16	23	-7	-7
17	9	-9	+7
18	3	-3	-3
19	1	-1	-1

Note that, for rounding, the average distortion in the number of events is independent of the number of bits removed. Also, for $n > 1$, the magnitude of the distortion is less for rounding compared to truncation.

To illustrate the effects of event count rounding and truncation, Table I has been populated with the expected number of events from an exact evaluation of (17) with $N = 495\,000$ and $s = 4.08$ for bins $k = 10{-}19$. Also given are the increases to N_e due to truncation and rounding when $n = 4$. In this instance, $L_{\rm et} + 1/2 = 16.835$ and $L_{\rm er} + 1/2 = 17.527$ mark the boundary beyond which the increases are no longer uniformly distributed, but instead, $\Delta N_e = -N_e$, i.e., the tails are trimmed.

This distortion can be considered a modification of the histogram by linearly combining it with a uniform distribution. In terms of a pdf, the resulting pdf, $p_{\rm lin}(v)$, is given by

$$p_{\rm lin}(v) = \frac{Np(v) + \Delta N p_u(v)}{N + \Delta N} \tag{21}$$

where N is the total number of events, prior to truncation, $p(v)$ is the pdf including the effects of ADC span and resolution, $\Delta N = (2L_e + 1)\langle \Delta N_e \rangle$ is the average increase in the number of events in the histogram, and $p_u(v)$ is a uniform pdf, ranging from $-L_e$ to $+L_e$. L_e and $\langle \Delta N_e \rangle$ are $L_{\rm et}$ and $\langle \Delta N_{\rm et} \rangle$ for truncation and are $L_{\rm er}$ and $\langle \Delta N_{\rm er} \rangle$ for rounding, respectively.

C. Kurtosis With Truncated Event Counts

We can evaluate the second and fourth moments of this linear combination distribution

$$m_2^{\rm lin} = \frac{N m_2^{\rm clip} + \Delta N \frac{L_e^2}{3}}{N + \Delta N} \tag{22}$$

$$m_4^{\rm lin} = \frac{N m_4^{\rm clip} + \Delta N \frac{L_e^4}{5}}{N + \Delta N}. \tag{23}$$

Then, the kurtosis is

$$R = \frac{(1 + \Delta N/N)\left(m_4^{\rm clip} + L_e^4 \Delta N/5N\right)}{\left(m_2^{\rm clip} + L_e^2 \Delta N/3N\right)^2} \tag{24}$$

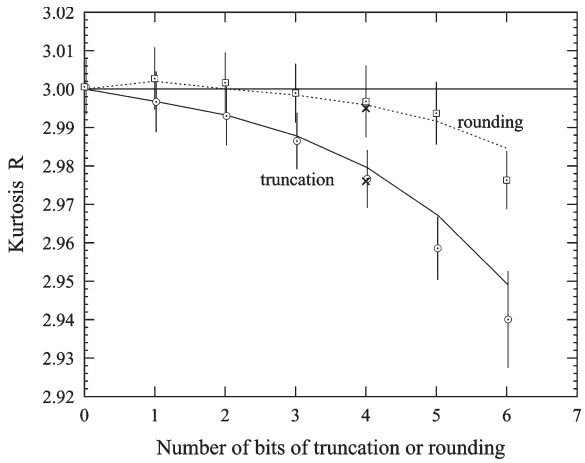

Fig. 6. Distortion of RFI-free kurtosis as a function of the number of bits of truncation or rounding in the reporting of histogram bin event counts. The curves are given by (24), and the open marks with error bars denote computer simulations. The X's mark the measurement mean. Upper data are for rounding; lower data are for truncation. $N = 495\,000$; $s = 4.08$; each point represents a run of 200 kurtosis simulations. The error bars represent one standard deviation of the kurtosis value.

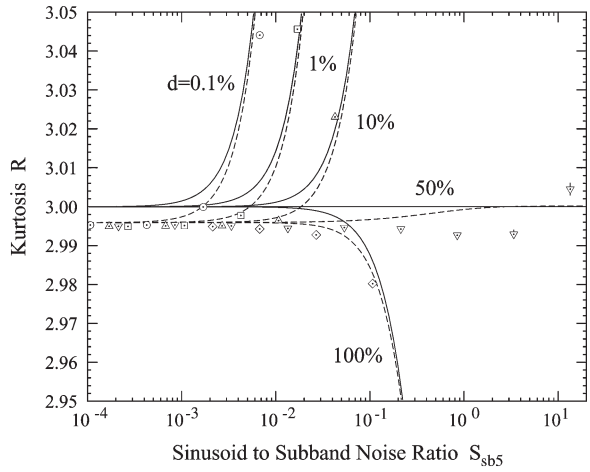

Fig. 7. Digitization-induced deflection of kurtosis with weak RFI. This plot is the same as Fig. 3, but zoomed in near $R = 3$. Solid curves are the kurtosis calculated from (5) and (6). The marks depict the mean kurtosis derived from measurements. Added to this plot are dashed curves from (24), which include the effects of event count rounding, tail trimming, and digitization. $N = 495\,000$; $s = 4.08$; $n = 4$.

where m_2^{clip} and m_4^{clip} are the second and fourth moments of $p(v)$ given by (15) and (16), respectively. Both components (tail trimming and event count distortion) contribute significantly to prediction of the mean value of the kurtosis.

Because the number of LSBs removed by the ADD firmware is fixed, we simulated the effect of varying n. Predictions of the mean value of the kurtosis match quite well with the computer simulations, as shown in Fig. 6. The kink in the curve for rounding at $n = 1$ is due to the fact that 0-bit rounding is no rounding or truncation at all. Both the simulations and (24) are close to the measured RFI-free kurtosis values for rounding and truncation at $n = 4$.

VIII. Deflection of Kurtosis in the Absence of RFI

For a large amount of interference, the interference is generally obvious, regardless of perturbations to the calculation of kurtosis. The analysis in the previous section for RFI-free kurtosis applies to kurtosis of an observation including a small amount of pulsed sinusoidal interference. This is because such a distribution is very close to an RFI-free distribution. Fig. 3 shows some measurements made in the laboratory for both large and small interference contributions. The model for the kurtosis in the absence of distortions is appropriate for the identification of RFI at this level. For the identification of low-level RFI, details of the behavior of the kurtosis near the value of three is important.

Fig. 7 shows a zoom in on data shown in Fig. 3 in the region near $R = 3$. The solid curves and the marks retain their meanings in these two figures. The inclusion of the dashed curves, which incorporate the effects of the removal of the LSBs from the histograms by ADD, demonstrates the improved ability to model the data at this scale. Thus, we have a chance of detecting the $d = 0.1\%$ RFI at $S = 2 \times 10^{-3}$, even though it produced a kurtosis value of three. For a radiometer with six subbands in the L-band radioastronomy window and $T_{\text{SYS}} = 600$ K, which roughly describes the benchtop radiometer, this corresponds to a detection of 0.2 K of RFI from an Air Route Surveillance Radar (ARSR-1), which operates with a similar duty cycle very close to the radio astronomy window [20].

IX. Conclusion

A laboratory demonstration of the ability of the kurtosis statistic to distinguish RFI-free radiometric observations from those contaminated with pulsed sinusoidal RFI is presented. The kurtosis statistic R value should be three for thermal noise because the noise obeys a Gaussian distribution. The kurtosis is useful for RFI detection because it may be higher than three for short-pulse RFI and may be lower than three for CW RFI. The use of a digitizer in the radiometer, which facilitates the calculation of the kurtosis, distorts the distribution from Gaussian due to several effects. Two of these distortions, namely, the quantization bin size and the span of the ADC, will be present in any digital radiometer back end. A third distortion, from the rounding of the number of events occurring in each quantization bin, is also present in this demonstration but need not be present in other systems. The effects of these distortions on the calculation of the kurtosis have been described. For a digitally calculated kurtosis to be insensitive to brightness, the rms noise voltage should be greater than three-fourths of the ADC resolution and less than 10% of the ADC span. These two conditions imply that the ADC should have at least 3 bits, with significantly improved performance at 4 bits or more. The kurtosis calculated with fewer ADC levels may still be useful for detecting some RFI. These results will find utility in translating radiometer interference requirements to digitizer specifications.

ACKNOWLEDGMENT

The authors would like to thank Prof. C. S. Ruf for the use of the ADD and CNCS and S. M. Gross for adding event count rounding to the ADD firmware.

REFERENCES

[1] D. M. Le Vine and M. Haken, "RFI at L-band in synthetic aperture radiometers," in *Proc. IEEE IGARSS*, Toulouse, France, Jul. 21–25, 2003, vol. 3, pp. 1742–1744.

[2] D. M. Le Vine, "ESTAR experience with RFI at L-band and implications for future passive microwave remote sensing from space," in *Proc. IEEE IGARSS*, Toronto, ON, Canada, Jun. 24–28, 2002, vol. 2, pp. 847–849.

[3] L. Li, E. G. Njoku, E. Im, P. S. Chang, and K. St. Germain, "A preliminary survey of radio-frequency interference over the U.S. in Aqua AMSR-E data," *IEEE Trans. Geosci. Remote Sens.*, vol. 42, no. 2, pp. 380–390, Feb. 2004.

[4] E. G. Njoku, P. Ashcroft, T. K. Chan, and L. Li, "Global survey and statistics of radio-frequency interference in AMSR-E land observations," *IEEE Trans. Geosci. Remote Sens.*, vol. 43, no. 5, pp. 938–947, May 2005.

[5] J. T. Johnson, A. J. Gasiewski, B. Güner, G. A. Hampson, S. W. Ellingson, R. Krishnamachari, N. Niamsuwan, E. McIntyre, M. Klein, and V. Y. Leuski, "Airborne radio-frequency interference studies at C-band using a digital receiver," *IEEE Trans. Geosci. Remote Sens.*, vol. 44, no. 7, pp. 1974–1985, Jul. 2006.

[6] S. W. Ellingson and J. T. Johnson, "A polarimetric survey of radio-frequency interference in C- and X-bands in the continental United States using WindSat radiometry," *IEEE Trans. Geosci. Remote Sens.*, vol. 44, no. 3, pp. 540–548, Mar. 2006.

[7] L. Li, P. W. Gaiser, M. H. Bettenhausen, and W. Johnson, "WindSat radio-frequency interference signature and its identification over land and ocean," *IEEE Trans. Geosci. Remote Sens.*, vol. 44, no. 3, pp. 530–539, Mar. 2006.

[8] M. Younis, J. Maurer, J. Fortuny-Guasch, R. Schneider, W. Wiesbeck, and A. J. Gasiewski, "Interference from 24-GHz automotive radars to passive microwave Earth remote sensing satellites," *IEEE Trans. Geosci. Remote Sens.*, vol. 42, no. 7, pp. 1387–1398, Jul. 2004.

[9] C. S. Ruf, S. Gross, and S. Misra, "RFI detection and mitigation for microwave radiometry with an agile digital detector," *IEEE Trans. Geosci. Remote Sens.*, vol. 44, no. 3, pp. 694–706, Mar. 2006.

[10] R. D. De Roo, S. Misra, and C. S. Ruf, "Sensitivity of the kurtosis statistic as a detector of pulsed sinusoidal RFI," *IEEE Trans. Geosci. Remote Sens.*, vol. 45, no. 7, pp. 1938–1946, Jul. 2007.

[11] M. G. Kendall and A. Stuart, *The Advanced Theory of Statistics*, 2nd ed., vol. 1. New York: Hafner, 1963.

[12] F. T. Ulaby, R. K. Moore, and A. K. Fung, *Microwave Remote Sensing: Active and Passive*, vol. 1. Reading, MA: Addison-Wesley, 1981.

[13] A. Papoulis, *Probability, Random Variables, and Stochastic Processes*, 2nd ed. New York: McGraw-Hill, 1984.

[14] S. O. Rice, "Statistical properties of a sine wave plus random noise," *Bell Syst. Tech. J.*, vol. 27, no. 1, pp. 109–157, Jan. 1948.

[15] M. Abramowitz and I. A. Stegun, *Handbook of Mathematical Functions*, ser. No. 55 in Applied Mathematics Series. Washington, DC: Nat. Bureau Standards, 1964.

[16] C. S. Ruf and J. Li, "A correlated noise calibration standard for interferometric, polarimetric, and autocorrelation microwave radiometers," *IEEE Trans. Geosci. Remote Sens.*, vol. 41, no. 10, pp. 2187–2196, Oct. 2003.

[17] R. H. Frater and D. R. Williams, "An active 'cold' noise source," *IEEE Trans. Microw. Theory Tech.*, vol. MTT-29, no. 4, pp. 344–347, Apr. 1981.

[18] R. D. De Roo, C. S. Ruf, and K. Sabet, "An L-band radio frequency interference (RFI) detection and mitigation testbed for microwave radiometry," in *Proc. IEEE IGARSS*, Barcelona, Spain, Jul. 23–27, 2007, pp. 2718–2721. Invited Session.

[19] M. A. Fischman and A. W. England, "Sensitivity of a 1.4 GHz direct-sampling digital radiometer," *IEEE Trans. Geosci. Remote Sens.*, vol. 37, no. 5, pp. 2172–2180, Sep. 1999.

[20] Federal Aviation Administration, *Spectrum Management Regulations and Procedures Manual*, May 1, 1998. FAA Order 6050.32A.

Roger D. De Roo (S'88–M'96) received the B.S. degree in letters and engineering from Calvin College, Grand Rapids, MI, in 1986, and the B.S.E., M.S.E., and Ph.D. degrees in electrical engineering from the University of Michigan, Ann Arbor, in 1986, 1989, and 1996, respectively. His dissertation topic was on the modeling and measurement of bistatic scattering of electromagnetic waves from rough dielectric surfaces.

From 1996 to 2000, he was a Research Fellow with the Radiation Laboratory, Department of Electrical Engineering and Computer Science, University of Michigan, investigating the modeling and simulation of millimeter-wave backscattering phenomenology of terrain at near grazing incidence. He is currently an Assistant Research Scientist with the Department of Atmospheric, Oceanic, and Space Sciences, University of Michigan. He has supervised the fabrication of numerous dual-polarization microcontroller-based microwave radiometers. His current research interests include digital correlating radiometer technology development, including radio-frequency-interference mitigation, and inversion of geophysical parameters such as soil moisture, snow wetness, and vegetation parameters from radar and radiometric signatures of terrain.

Sidharth Misra received the B.E. degree in electronics and communication engineering from the Nirma Institute of Technology, Gujarat University, Ahmedabad, India, in 2004, and the M.S. degree in electrical engineering and computer science from the University of Michigan, Ann Arbor, in 2006. He is currently working toward the Ph.D. degree in the Department of Atmospheric, Oceanic, and Space Sciences, University of Michigan.

He was a Research Engineer with the Space Physics Research Laboratory, University of Michigan, where he worked on the analysis and implementation of the agile digital receiver for radio-frequency-interference (RFI) mitigation. He has also worked on Oceansat-II for the Space Applications Center, Indian Space Research Organization, Ahmedabad, India. He was a Research Assistant with the Danish National Space Center, Technical University of Denmark (DTU), Lyngby, Denmark, where he performed RFI analysis for CoSMOS, an airborne campaign preparing for SMOS at DTU. His research interests include signal detection and estimation, filter design, and image processing.